International Journal of Science and Engineering Invention (IJSEI)
Volume 10, Issue 10, December 2024
https://doi.org/10.23958/ijsei/vol10-i10/276

Original article

Multi-Response Optimization of Stir Casting Parameter of New Nanocomposites Formulation of Al-Si-Mg Alloy Reinforced with Synthesis Carbon Nanotube and Periwinkle Shell Nanoparticles via Taguchi-Grey Approach

Vincent Chukwuemeka Ezechukwu *[1], Tamunonimim Kelsy Braide [1], Chukwuemeka Chidozie Nwobi-Okoye [2]

[1]Doctor of Philosophy, Department of Mechanical Engineering, Chukwuemeka Odumegwu Ojukwu University, Anambra State Nigeria.
[2]Professor, Department of Mechanical Engineering, Chukwuemeka Odumegwu Ojukwu University, Anambra State Nigeria.

*Corresponding author: Vincent Chukwuemeka Ezechukwu; *vc.ezechukwu@coou.edu.ng*

Received 23 October 2024; Accepted 30 November 2024; Published 04 December 2024

Abstract

The optimal parameter settings for stir casting of the A-Si-Mg alloy reinforced with carbon nanotubes synthesized from rice husk (CNTs -derived RH) and periwinkle shell nanoparticle (PWSnp) nanocomposites were determined using the Taguchi-grey relational method. The wt% CNTs derived RH, wt% PWSnp stirring speed, and time were the stir casting parameters, and porosity, hardness values, and compressive strength were used in the multi-response for the study. The optimal condition is 0.5wt CNTs derived RH, 1.5wt% PWSnp, 250rpm stirring speed, and 5-minute stirring time. The Taguchi Grey method is applicable for the multi-response optimization of aluminum waste beverage cans, CNTs derived from RH, and PWSnp nanocomposites, as the experimental results fall within the range of the predicted values.

Keywords: ***Stir Casting Parameters, Al-Si-Mg Alloy, Carbon Nanotubes (CNTs) Derived from Rice Husk, Periwinkle Shell Nanoparticles (PWSnp), Taguchi-Grey Relational Method, Nanocomposites Optimization.***

1.0 Introduction

The enhancement of aluminum metal matrix composites (AMMCs) is influenced by several factors, including the fabrication method, the characteristics of the reinforcements, the proportion of the reinforcements, the size of the reinforcing particles, and the distribution of the reinforcing phase [1]. When compared to micro-sized reinforcements, it was shown that Nano-sized reinforcements give the matrix better mechanical, tribological, thermal, and electrical qualities [2]. This is because it has been established that they have increased surface area, shorter diffusion distances, and increased grain boundary atom [3].

Reinforcement of metal alloys with Bio-Nano particles, bio fibers, and bio whiskers has taken centre stage in research and innovation [4]. However, the interest in using biodegradable, biocompatible, and bioresorbable nanomaterials is justified by the fact that they are degradable and can be metabolized by the body without causing havocs [5]. The use of conventional and inorganic nanomaterials as reinforcements for metal matrix composites can be costly and dangerous to health; so, researchers are now more focused on the reinforcement of AMMCs using low-cost biomaterials from plants and animals. Biomaterials not only reduce the cost but also the weight of the composite, thereby, conserving energy and making it more useful to aerospace and automotive applications [1].

Stir casting is the cheaper means of producing AMCs. The method can be used for the large production of simple and complex shapes AMCs. The stir casting method has been used in the production of AMC's using and suitable PKSnp [1], NiTi [6], Si3N4 [7], CNTs [8], TiN [9] Al2O3 [10], TiC [11], and Ni [12]. Numerous techniques have been used to enhance the wetting of stir-casted composites, which include raising the surface energy of the dispersoids, lowering the surface tension of the liquid matrix, and reducing the solid-liquid interfacial energy of the matrix reinforcement [13]. Now, it has been established that the dispersoid surface is usually enclosed with a gas layer which prevents the homogenous mixing of the matrix and reinforcement. Also, if the

quantity of the dispersoid present in the matrix melt gets to a certain level (critical level), the gas layers form a barricade resulting in a complete rejection of the dispersoids from the melt [14]. So, these barricading gases must be dissolved before or during stir casting of the metal matrix composites [15]. Hence the study of the processing parameter of stir casting is very imperative in the development of AMMCs.

CNTs were chosen as one of the reinforcements because of their peculiar striking properties. It has low CTE, a high modulus of elasticity, low density, and high thermal and electrical conductivities. Hence, the choice is justifiable as it will impart all these properties unto all alloys. The CNTs will be synthesis from rice husk because Ngu *et al* [16] developed CNTs from rice husk for optical sensing of metal ions application.

Waste beverage can be used as a source of aluminum because Asafa *et al* [17] Potentials of composites using Discarded Aluminum Based and Snailshell. Daiwa *et al* [18] evaluated the properties of pumice and recycled beverage cans. Also, periwinkles shell nanoparticles will be used in this work, because the use of periwinkles shells as reinforcement materials in AMMCs has been well documented in the literature. Ezechukwu *et al* [19] reported on composite material using hybrid of momordica angustisepala fiber and breadfruit seed shell ash particles. Umunakwe *et al* [20] developed a periwinkle shell and aluminum 6063 composites. From the literature, it was observed the development of hybrid nanocomposites using waste beverage can, periwinkle shell nanoparticles, and CNTs derived from RH has not been giving much attention. This work will report for the first time the stir casting parameter on the properties of waste aluminum can reinforced periwinkle shell nanoparticles and CNTs derived from RH using the Taguchi grey approach since the proper selection of process parameter dedicate the properties obtain of the composites because stir casting product can be susceptible to poor distribution of reinforcement, microporosity, and interfacial reaction.

2.0 Materials and Method

2.1 Materials

The periwinkles shell used in this work was obtained in the Port Harcourt River State Nigeria, while that rice husk waste was obtained in Ebonyi State Nigeria

2.2 Method

2.2.1 The production of the CNTs from the rice husk waste

The production of the CNTs from the rice husk waste followed the method adopted in which the process used to produce the CNTs from the rice husk waste involved washing and drying the RH to get rid of any contaminants. After being cleaned, the RH was dried for 24 hours at 65 degrees Celsius. The dehydrated RH was crushed into RH powders and sieved until it was 25µm in size. After dissolving ferrocene, Fe(C5H5)2, as a catalyst in ethanol, the dried RH was added. A sheet of metal was used as the substrate for the combination. The samples were placed in the middle of the quartz tube within the Samsung M539 MAN200405W microwave oven, which had a power output of 600W and a frequency of 2.45GHz (home microwave frequency). The quartz tube was evacuated to a base pressure of 1.3 × 103 mbar prior to microwave plasma irradiation. The duration of the deposition was 40 minutes.

2.2.2 Synthesis of Nano-Calcium Oxide from Waste Periwinkle shell (PWSnp) The sol-gel method was used in the production of the PWSnp. The periwinkle shell (PWS) serves as the precursor. The PES Waste was washed with deionized water. The cleaned PWS was dried at a temperature of 120oC for a period of 2 h and ground using pulverized using a ball milling machine at speed of 250rpm and were sieved to a particle size of 50µm. About 25g of the ground PWS was dissolved in 500 ml in 1Mhydrochloric acid (HCl) to obtained calcium chloride (CaCl2) by equation 1[21].

$$(PWS)CaCO3\ (s) + 2HCl\ (aq) \text{----} CaCl_2\ (aq) + H_2O\ (l) + CO_2\ (g) \quad (1)$$

The production of 'sol' was then obtained by hydrolysis process. In the hydrolysis process, 250 mL of 1 M sodium hydroxide (NaOH) was added drop by drop to transformed the $CaCl_2$ into a gel (see equation 2).

$$CaCl_2\ (aq) + 2NaOH\ (aq) \text{------} Ca(OH)_2\ (s) + 2NaCl\ (aq) \quad (2)$$

The gel Ca(OH)2 formed will be aged for 24 hours at ambient temperature and filtration followed. The filtrate will be cleaned using distilled water to remove impurities in the precipitate, drying of the synthesized gel will be done in Oven at 65°C for 12 hours followed by calcined in a muffle furnace at a temperature of 850°C for 2 hours (equation 3) [21].

$$Ca(OH)_2\ (s) + Heat \text{----------} CaO\ (s) + H2O \quad (3)$$

2.2.3 Taguchi experiment design

Taguchi-grey experiment design was used for modeling the effect process parameters on the hardness values, porosity, and compressive strength Taguchi's methods focus on the effective application of engineering strategies rather than advanced statistical techniques. It includes both upstream and shops floor quality engineering. Taguchi's approach to parameter design provides the design engineer with a systematic and efficient method for determining near-optimum design parameters for performance and cost. The wt% CNTs derived RH(A), wt % PWSnp (B), stirring speed(C), and stirring time (D) were the selected casting factors considered in this work. Table 1 was displayed the factors and the levels used in the work. This was made possible from the preliminary experiments.

Table 1: Stir casting parameters and their values at a different level

Process parameters	Low (1)	Medium (2)	High (3)
Wt % CNTs derived RH(A),	0.5	1.0	1.5
Wt % PWSnp (B)	0.5	1.0	1.5
stirring speed(C) rpm	100	200	300
Stirring time(minutes)	2	4	6

2.2.4 Sample Production

The samples were produced as per Taguchi's approach of L9 using the Stir casting parameters and their values at a different level as displayed in Table 1. The liquid method of the metal matrix was used in the production. This liquid method is cheaper and reliable compared with another method. The cleaned calculated amount of aluminum beverage, 7w% Si, and 0.3wt% Mg to formed A356 alloy were placed inside a graphite crucible and heated to a temperature of 750oC. The reinforcement particles were preheated in Table 1 before incorporation into the melt to improve wettability and harmonize the temperature. After the molten metal was fully melted, degassing tablets (hexachloroethane) were added to reduce porosity.

A stirrer was done using stainless steel coated graphite, the stirrer was lowered into the melt slowly to stir the molten as per Table 1. 0.3wt%magnesium was added to the melted. Then preheated reinforcement was then added to the molten metal. The mixture was then poured into a mold preheated to 500oC for 30 min to obtain uniform solidification (**Figure 1**). After casting, the sample was machined to determine of physical and mechanical properties.

Figure 1: a) Pouring of the molten composites inside the mold b) Mould filled with molten composites c) Composites samples produced.

2.2.5 Characterization of the Nanocomposites

The apparent porosity of the samples was determined as per ASTM C830-00[22] using equation 4.

$$A.P\% = \frac{ws-wd}{ws-wi} \times 100\% \quad (4)$$

Where: WD = dry weight, WS = soaked weight, WI = immersed weight, A.P% is apparent. The evaluation of the mechanical behavior of a sample under compression loading is important for component design and service performance assessment. The compressive strength was done as per ASTM D3410 / D3410M-16e1[23] using a Testometric Machine. The Vickers Micro-hardness tester was used to determine the hardness. The hardness test was done as per ASTM E92-17 [24]. The samples were being grounded and polished mechanically and etched with Keller's Agent (2 ml HF, 20 ml HNO3, and 175 ml distilled water. JOEL JSM 5900 scanning electron microscope was used to determine the microstructure as per ASTM E986-04 [25].

3.0 Results and Discussion

3.1 Chemical Composition of the PWSnp

The result chemical analysis of the PWS and PWSnp by XRF is displayed in Table 4.3. it was observed in Table 2 that CaO is the main compound in the PWS and PWSnp. However, the amount of CaO in the PWSnp is greater than in the PWS, and also the PWS has a high amount of loss of ignition. This could be attributed to the fact that in calculations the $CaCO_3$ in the PWS is converted to CaO and CO_2. This result is on par with the work of Abdelmalik and Sadiq [26].

Table 2: XRF analysis of PWSnp

%	CaO	Na_2O	SiO_2	Al_2O_3	MgO	MnO	P_2O_5	Fe_2O_3	TiO_2	Loss of ignition
PWS	49.59	0.08	0.01	0.01	0.04	0.01	0.34	0.01	0.02	49.89
PWSnp	89.78	1.05	0.03	0.03	0.13	<0.01	0.45	0.04	0.01	8.47

3.2 Microstructure of PWSnp and wt% CNTs derived RH

The microstructure of PWSnp and wt% CNTs derived RH is displayed in Figure 2. The microstructure of the PWSnp shows spherical shapes in polycrystalline character (**Figure 2b**). This structure obtained for the PWSnp is in confirmation with the CaO formed in eggshell [27]. The average particles obtained for the PWSnp were 98nm. The TEM image shows the multi-walled carbon nano-structure. The nanocluster, web-like network, several nanometers long was displayed in Figure 2b. The average particle size obtained in the TEM image ranges from 45-75nm. This is on par with other nanostructures produced from rice husk by Muhammad Asnawi [28].

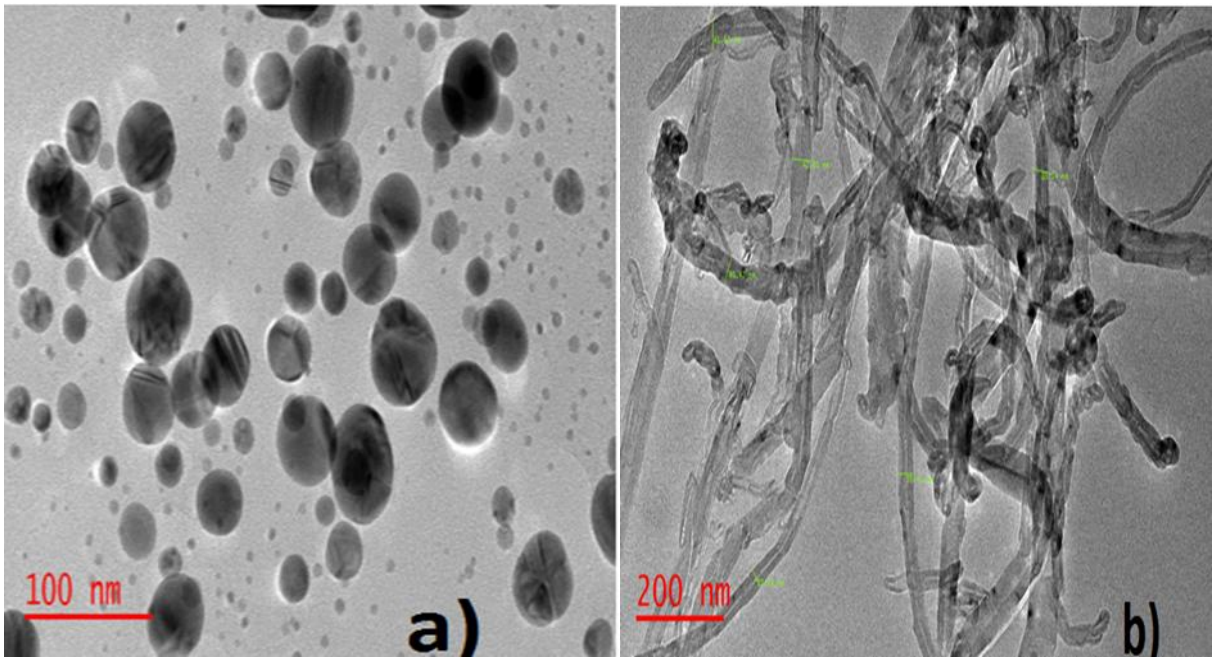

Figure 2: a) TEM image of PWSnp b) TEM image of the CNTs derived RH

3.3 Multi-response optimization (Grey Analysis)

Grey relational analysis was used to determine the optimum parameter setting that gives the higher compressive strength, higher hardness values, and lower porosity. The results of the multi-response from the Taguchi L9 are displayed in Table 3. Hence there is the need to obtain a unified optimum setting that will represent the three-output characterization using equation 5 for smaller for better for porosity output characterization and higher the better for compressive strength and hardness values equation 6 for i.e $0 \leq S/N \leq 1$

$$X_i(k) = \frac{max\, X(k)_i - X(k)_i}{max\, X_i(k) - min\, X(K)_i} \quad (5)$$

$$X_i(K) = \frac{X_i(K) - min\, X(K)_i}{max\, X - min\, X_{Ii}(K)} \quad (6)$$

where) and refer to the sequence after data pre-processing and the comparability sequence, respectively, and k = 1 for i = 1. 2. 3. ... for experiment numbers 1 to 9. The results of the grey relational generation and deviation are displayed in Table 4.

The deviation sequence of the reference sequence and the comparability sequence will be calculated using Equation 7:

$$\Delta_{0i}(k) = |x_0{}^x(k) - x_i{}^x(k)| \quad (7)$$

Table 3: Results of the Taguchi experiment(L9)

S/No	%wt CNTs	%wt PWSnp	Stirring speed	Stirring time	Porosity (%)	Hardness Values (HV)	Compressive strength (MPa)
1	1	1	1	1	0.12	87.56	245.67
2	1	2	2	2	0.12	89.01	268.23
3	1	3	3	3	0.15	91.50	289.45
4	2	1	2	3	0.18	98.32	345.78
5	2	2	3	1	0.25	99.26	367.8
6	2	3	1	2	0.34	97.90	355.89
7	3	1	3	2	0.3	105.89	401.89
8	3	2	1	3	0.290	116.8	410.67
9	3	3	2	1	0.30	100.89	398.76

The grey relational coefficients (GRC) were determined for the output characteristics using equation (8).

$$\zeta_1(K) = \frac{\Delta_{mm} + \zeta\Delta_{max}}{\Delta_{0i}(k) + \zeta\Delta_{max}} \quad (8)$$

where Δoi(k) is the determined deviation obtained from the normalized S/N value, while was the is the Δmax maximum normalized S/N ratios values for each of the three output characteristics and is which is usually 1 and Δmin minimum normalized S/N ratios values for each of the three output characteristics, ξi(k) is the grey relational coefficient, ξ is the distinguishing or identification coefficient which lines within $0 \leq \xi \leq 1$, and ξ equal to 0.5 was adopted in this research.

The GRG is determined by averaging the GRC corresponding to each performance characteristic. The overall evaluation of the multiple performance characteristics is based on the GRG. as presented in Equation 9,

$$r_1 = \frac{1}{n}\sum_{k=1}^{n} \zeta_1(k) \quad (9)$$

Where Yi refers to the GRG for the Ath experiment, while n reflects the number of performance characteristics. Therefore, a higher GRG showed that the corresponding experimental result was closer to the ideally normalized value. The results of the GRC and GRG are displayed in Table 5.

Table 4: Grey relational generation and deviation

S/NO	Grey relational generation			DOI		
	Hardness values	Compressive strength	porosity	Hardness values	Compressive strength	porosity
1	**0**	**0**	**1**	**1**	**1**	**0**
2	0.049589603	0.136727273	**1**	0.950410397	0.863272727	**0**
3	0.134746922	0.265333333	0.863636364	0.865253078	0.734666667	0.136363636
4	0.367989056	0.606727273	0.727272727	0.632010944	0.393272727	0.272727273
5	0.400136799	0.740181818	0.409090909	0.599863201	0.259818182	0.590909091
6	0.353625171	0.668	**0**	0.646374829	0.332	**1**
7	0.626880985	0.946787879	0.181818182	0.373119015	0.053212121	0.818181818
8	**1**	**1**	0.227272727	**0**	**0**	0.772727273
9	0.455882353	0.927818182	0.181818182	0.544117647	0.072181818	0.818181818

Table 5: Grey relational coefficient and Grey Relational Grade (GRG)

S/NO	Grey relational coefficient			Grey Relational Grade (GRG)
	Hardness values	Compressive strength	Porosity	
1	0.75	**0.75**	**0.25**	0.583333333
2	0.725205198	0.681636	**0.25**	0.552280521
3	0.682626539	0.617333	0.318181818	0.539380564
4	0.566005472	0.446636	0.386363636	0.466335157
5	0.549931601	0.379909	0.545454545	0.491765079
6	0.573187415	0.416	0.75	0.579729138
7	0.436559508	0.276606	0.659090909	0.457418826
8	0.25	0.25	0.636363636	0.378787879
9	0.522058824	0.286091	0.659090909	0.489080214

3.3.1 Grey relational grade diagram

Figure 3 displayed a grey relational grade diagram and the middle line gives the grey relational grade mean. The wt% CNTs derived RH has the greater grey relational grade affecting the porosity, hardness values, and compressive strength. Increasing the wt% wt% CNTs derived RH from level 1(0.5) to level 3(1.5) decreased grey relational grade, however increasing the stirring speed from level 1 to level 3 increases the grey relational grade. The increment in the grey relational grade with increases in the stirring speed affect the distribution and of the reinforcement and resulted in a reduction in porosity. The lower the string speed results in a poor distribution of the particles. Increment in stirring speed to rise the centrifugal current inside the aluminum matrix melt and leads to disintegrates the reinforcement clusters into uniformly distributed particles. The grey relational grade increases from level 1 to level 2 and then decreased in level 3. The reduction of grey relational grade as the stirring time increased to level 3 may be attributed to a long time of stirring that may lead to the molten metal solidification and lead to the weak interfacial bonding between the metal and the reinforcement. However, the grey relational grade decreased to level 2 and later increases to level 3 as the wt% PWSnp increase.

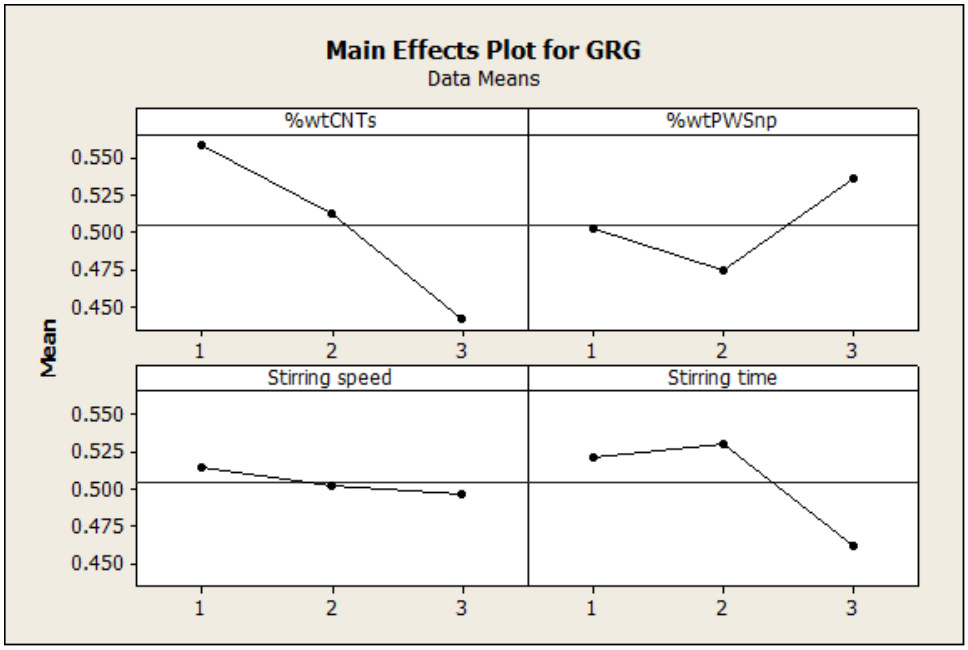

Figure 3: Grey relational grade diagram

3.3.2 Analysis of Response Surfaces.

Figure 4a-4e was used to further discuss the effect wt% CNTs derived RH, wt% PWSnp, stirring speed, and stirring time on the hardness values, compressive strength, and porosity of the composites. It was observed from Figure 4a-4b that the higher hardness values, compressive strength, and lower porosity were

registered as the influence of the minimum level of wt% CNTs derived RH and middle level of stirring time. The highest significant effect of stirring time and stirring speed in the hardness values, compressive strength, and porosity of the composites was observed in Figure 3c-3d. The effect in the reduction of the hardness values, compressive strength, and higher porosity from 1 to +3 levels as the wt% CNTs derived RH has been discussed in Figure 4a-4b. The high hardness values and compressive strength obtained in the composite samples help to increase the load-bearing capacity of the composite materials. Similar enhancement has been noted in the literature [29]. Interaction plot represents interaction effect of control factor on performance characteristics, showing the maximum value of hardness values, compressive strength and porosity hardness values, compressive strength, and minimum porosity at the interaction of 0.5wt CNTs derived RH, 1.5wt% PWSnp, 250rpm stirring speed, and 5minutes stirring time (**Figure 4e**).

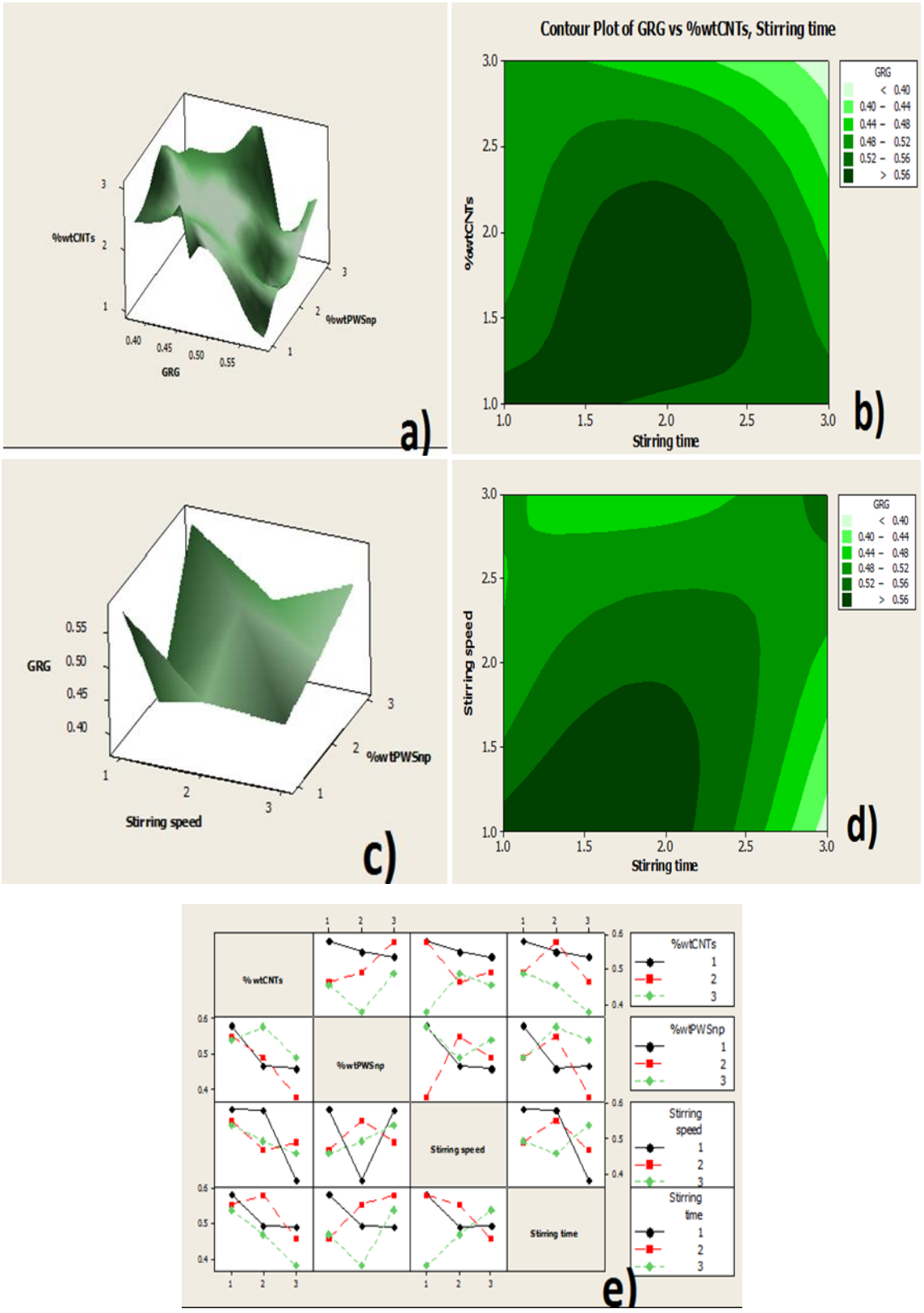

Figure 4: a) 3D plot of GRG with wt% CNTs derived RH and wt% PWSnp b) Contour plot of GRG with wt% CNTs derived and stirring time c) 3D plot of GRG with stirring speed and wt% PWSnp d) Contour plot of GRG of stirring speed and stirring time e) Interaction plot of GRG with the four factors

3.3.3. Analysis of Variance results

Table 6 presented the ANOVA results obtained in this study. The ANOVA analysis was done at a low level of F-test of 0.0002. It was observed that an F-value of 24.32 was obtained in this work means the model under investigation is significant. The wt% CNTs derived RH(A) is the only factor under investigation that is significant since the P-value obtained is less than 0.0.05000. A value of 0.9865 obtained for the Pred R-Squared was close to 00.9459 for the Adj R-Squared with 0.50 as mean values and 0.066 as standard deviation. The ANOVA analysis indicates that the model has both statistical and physical significance (percentage contribution > error) in the wear behavior of the composites coating. The developed model has good significance since the R-value obtained is close to 1.

Table 6: ANOVA for the GRG

Source	Sum of squares	DF	Sum of men	F	P	
Model	0.035	6	5.807E-003	24.32	0.0400	Significant
wt% CNTs derived RH	*0.021*	2	*0.010*	*43.39*	*0.0225*	
Wt% PWSnp	*5.780E-003*	2	*2.890E-003*	*12.10*	*0.0763*	
Stirring time	*8.339E-003*	2	*4.169E-003*	*17.46*	*0.0542*	
Residual Error	4.776E-004	2	2.388E-004			
Total	0.035	8				

3.3.4 Mathematical modeling

The work-developed model equation was used to study the correlation coefficient. The analysis was done using the design expert 9 software. Equation 10 displayed the correlation equation obtained for this work.

GRG =+0.50+0.054* A[1]+8.222E-003 * A[2]-1.778E-003* B[1]-0.030* B[2] +0.017 * D[1] +0.026 * D[2] (10)

It was seen clearly in equation 2 that the coefficient associated with wt% CNTs derived RH(A) stirring time(D) is positive. While the coefficient associated with the wt% PWSnp (B) is negative. The wt% CNTs derived RH addition has the highest regression coefficient value (0.054) for GRG. This was used to support the ANOVA result that wt% CNTs derived RH has a greater effect on the GRG.

The residual plot for the analysis is presented in Figure 5. It was observed that the experimental value is close to that of the predicted values since the points are randomly distributed close to the line in the plot. This was used to supports the earlier conclusion that the model is significant. To actual confirm the model; nine (9) set of experimental conditions was used for the design. The results are displayed in Figure 6. From Figure 6 most of the experimental values are within the limit of predicted values; few were nearer and crossed the predicted values.

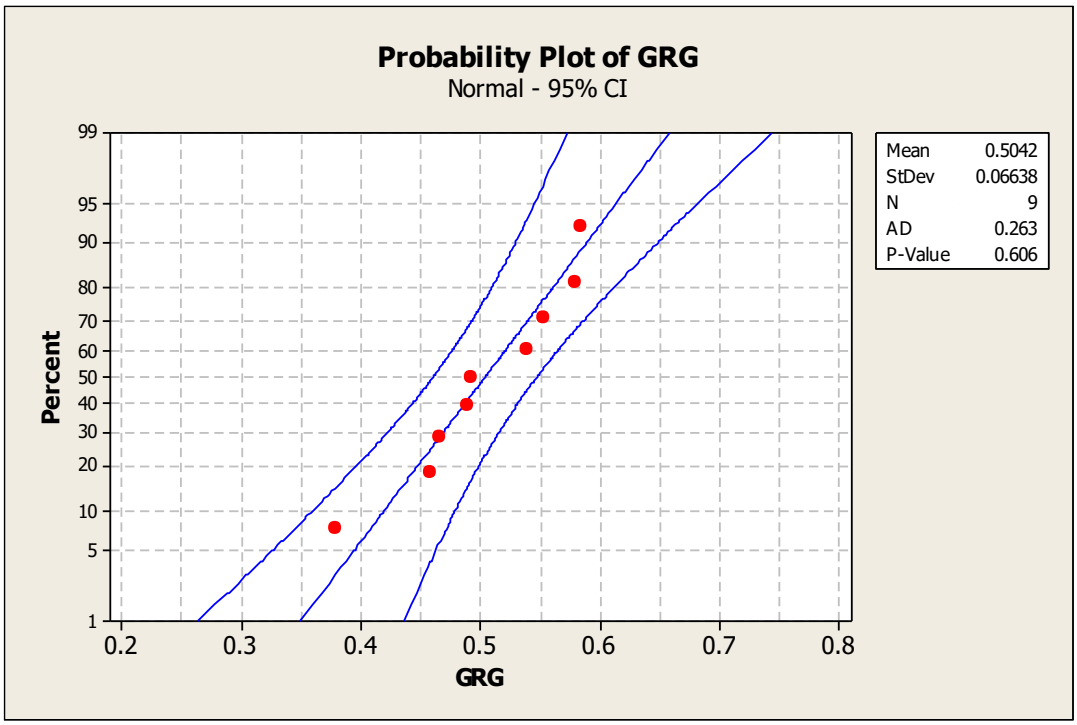

Figure 5: Residual plots for wear rate

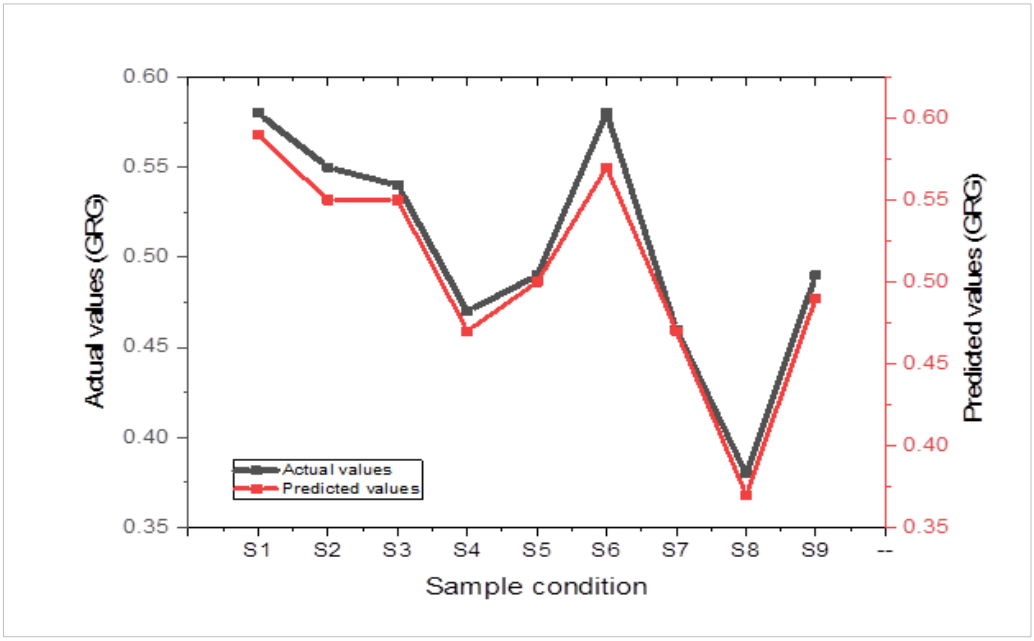

Figure 6: Validation of the mathematical model

3.3.6 Optimal Setting

The mean of the GRG is used as a correlation between the comparability sequence of GRG and the reference sequence. The greater the GRG shows a high correlation. From Table 7, A1B3C1D2 (%wt CNTs derived RH level 1, wt% PWSnp level 3, stirring speed level 1, and stirring time level 2) gives the optimal setting of the GRG. The grades in the response Table serve as a measure of the rank. In Table 7 %wt CNTs derived RH has the highest effect on the hardness values, porosity, and compressive strength and is rank 1 with the greater delta value 0.1166, followed by the stirring time rank 2 with 0.0683 as delta value, wt% PWSnp rank 3 with a delta value of 0.0618 and stirring speed rank 4 with 0.0178 as delta value. Hence the optimal condition is 0.5wt CNTs derived RH, 1.5wt% PWSnp, 250rpm stirring speed, and 5minutes stirring time

Table 7: Response Table for Means

Level	%wt CNTs (A)	%wt PWSnp (B)	Stirring speed(C)	Stirring time(D)
1	0.5583[x]	0.5024	0.5140 [x]	0.5214
2	0.5126	0.4743	0.5026	0.5298[x]
3	0.4418	0.5361	0.4962	0.4615
Delta	0.1166	0.0618 [x]	0.0178	0.0683
Rank	**1**	**3**	**4**	**2**

The optimum GRG was computed from equation 11.

$$GRG = AVR_{ORG} + (wt\%CNTs - derived_{opt}RHAVR_{org}) + (wt\%PWS_{np} - AVR_{GRG}) + (Stir - speed_{opt} - AVR_{ORG}) + (stir - time_{opt} - AVR_{GRG} \quad (11)$$

Where, expected response (GRG), average GRG(AVR), mean response at A1B3C1D2 setting condition.

GRG=0.5 + (0.5583 -0.5) + (0.5361 -0.5) + (0.5140 -0.5) + (0.5298-0.5), GRG= 0.5 + 0.0583 + 0.0361+0.014 +0.0298, GRG= 0.638 (Table 8)

Table 8: Optimum Levels of Process Parameters

Process parameter	Parameter designation	Optimal level	GRG	
Wt% CNTs derived RH	A	L1 (0.5wt %)	Prediction	Experiment
Wt% PWSnp	B	L3 (1.5wt %)	0.638	0.583
Stirring speed	C	L1 (10orpm)		
Stirring Time	D	L2 (4minutes)		

3.4 Microstructure confirmation

The microstructure of the sample was further used to confirm the effect of the casting parameter on the hardness values, compressive strength, and porosity of the cast composites. The addition of the reinforcement leads to the decreases of the grain size because the reinforcement causes hinder grain boundaries (**compare Figure 7a with 7b**) and heterogeneous nucleation occurring due to the addition of 0.5wt%CNTs derived RH and 1.5wt% PWSnp. The reinforcement was uniformly distributed in the aluminum matrix. The modified stir-casting method used in the production of the novel composites was able to avoid agglomeration and clusters of the particles. The reinforcement has a round and ellipsoidal shape. The particles are seen clearly as dark phases within the aluminum grain. The microstructure shows that good interfacial bonding exists between the reinforcement and the matrix when the level of CNTs derived RH and PWSnp are within the optimal setting. However higher content of CNTs derived RH in the formulation leads to agglomeration and porosity (**Figure 7c**), this is used to support the earlier conclusion that higher content of 0.5wt% CNTs derived RH create more porosity, lower hardness values, and compressive strength. A similar observation has been observed in the work of Selvan *et al* [30].

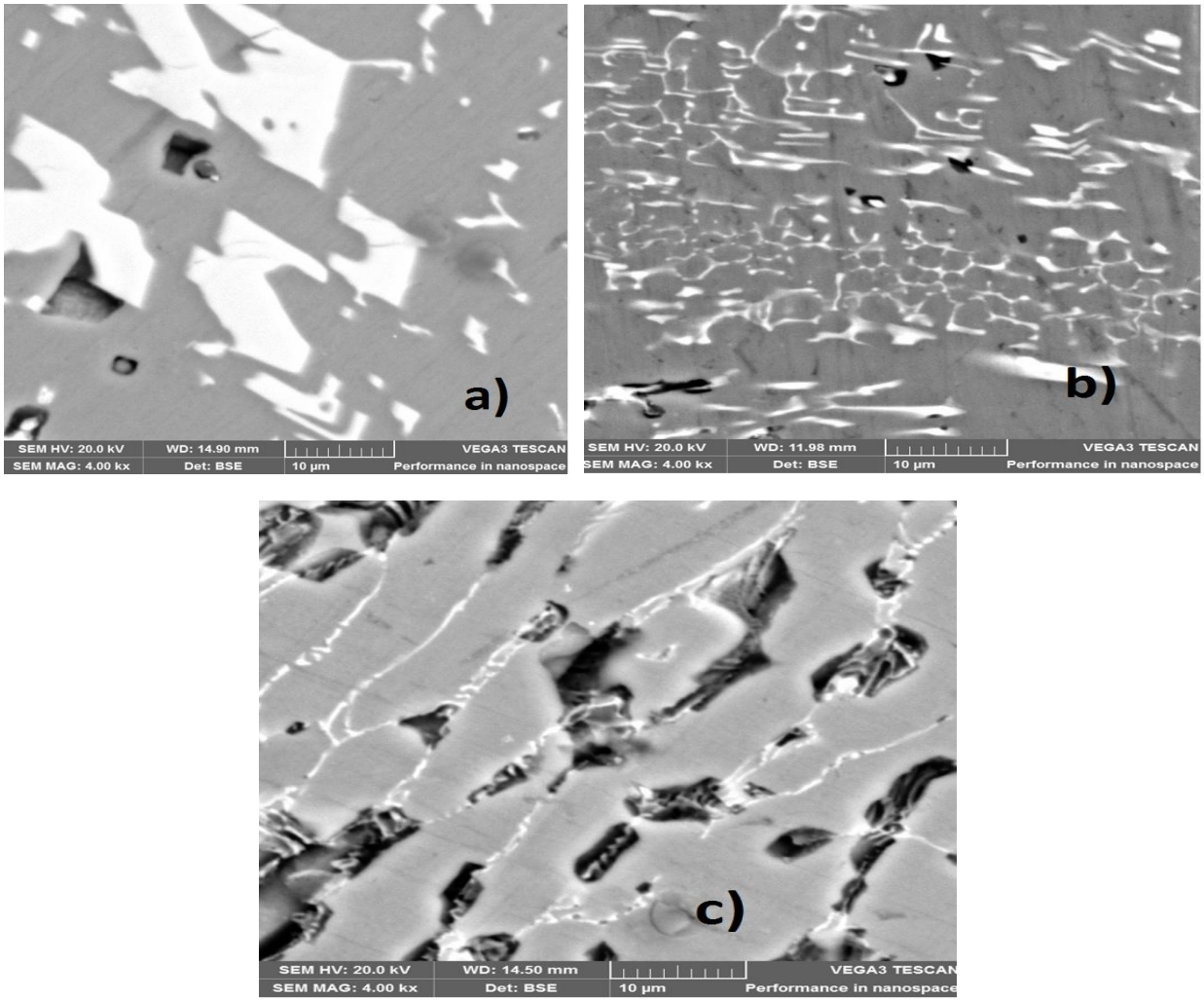

Figure 7: SEM image: a) Aluminum alloy b) optimal condition (0.5wt% CNTs derived RH and 1.5wt% PWSnp) c) 1.5wt% CNTs derived RH and 1.5wt% PWSnp

The study of the interface and boundaries between the matrix and the reinforcement was done for the optimal sample using a transmission electron microscope (TEM). The TEM image is displayed in **Figure 8**. It was observed that there was fine and uniform distribution of the reinforcement with the aluminum grain boundary. There was high dislocation density observed within the interface and boundaries between the matrix and the reinforcement, a coherent interface with a regular arrangement of the reinforcement was seen. The crystal structure was determined using TEM, the reinforcement has a=2.464 Å, b=2.464 Å, C= 7.660 Å, α=90o, β=90o and γ=120o with d1002(Hexagonal) crystal structure and dislocation density of 2.69g/cm3., while the α-Al have a=4.0494 Å, b=4.0494 Å, C= a=4.0494 Å, α=90o, β=90o and γ=90o with dislocation density of 2.56gcm3 and d111cubic structure. The mismatch between the reinforcement and the matrix at the interface was 4.83%.

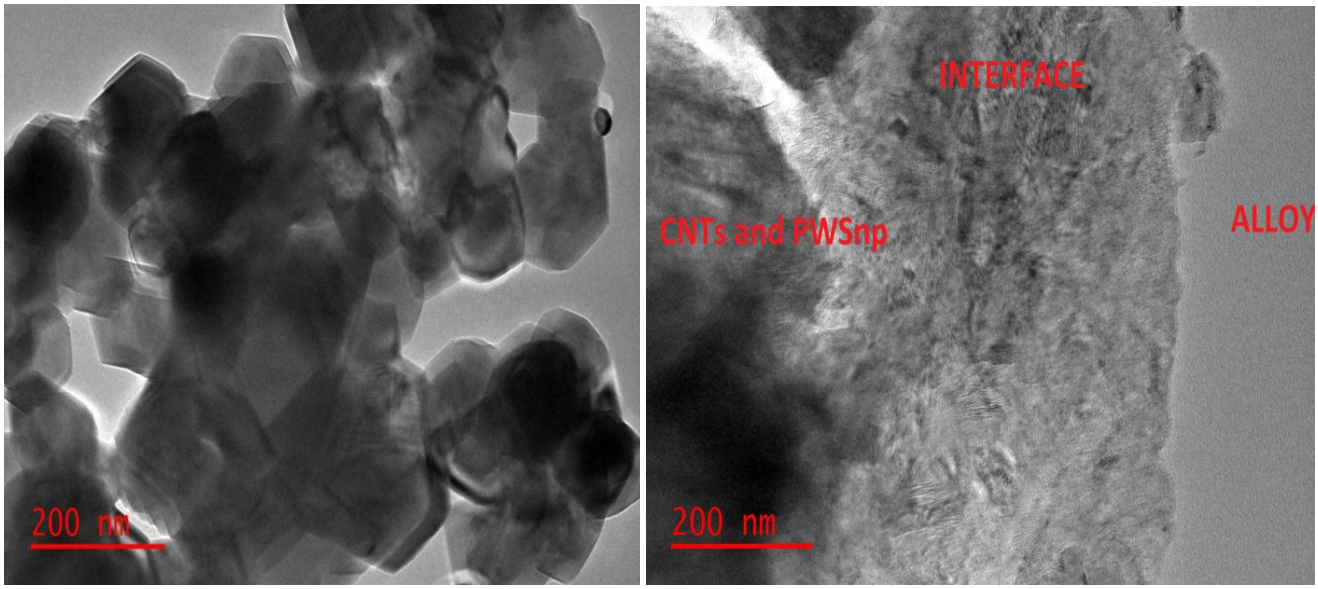

Figure 8: a) TEM image of composite at optimal setting, b) Fast Fourier transform of the region

4.0 Conclusions

The multi-response optimization of nanocomposites produced using aluminum waste beverage can, CNTs derived RH and PWSnp was an investigation. In the course of the study, the following new information and conclusions are made:

1. The optimal condition is 0.5wt CNTs derived RH, 1.5wt% PWSnp, 250rpm stirring speed, and 5minutes stirring time.
2. Good interfacial bonding exists between the reinforcement (CNTs derived RH and PWSnp) at the optimal setting.
3. The mismatch between the reinforcement and the matrix at the interface was 4.83%.
4. The Taguchi Grey approach can be used in multi-response optimization of aluminum waste beverage can, CNTs derived RH, and PWSnp nanocomposites since the experimental values are within the limit of predicted values.

References

[1] Braide, T.K., Nwobi-Okoye, C.C. & Ezechukwu, V.C. Taguchi-Grey multi-response optimization of wear parameter of new nanocomposite formulation of Al-Si-Mg alloy reinforced with synthesis carbon nanotube and periwinkle shell nanoparticles. Int J Adv Manuf Technol 120, 8363-8375 (2022). https://doi.org/10.1007/s00170-022-09163-7

[2] Braide T. Kelsy, Chidozie Chukwuemeka Nwobi-Okoye, Vincent Chukwuemeka Ezechukwu, Remy Uche, Multi-objective optimization of novel Al-Si-Mg nanocomposites: A Taguchi-ANN-NSGA-II Approach, Journal of Engineering Research,2023, ISSN 2307-1877, https://doi.org/10.1016/j.jer.2023.10.008.(https://www.sciencedirect.com/science/article/pii/S2307187723002687)https://doi.org/10.1016/j.jer.2023.10.008. (https://www.sciencedirect.com/science/article/pii/S2307187723002687)

[3] Ahamed, A.A., Ahmed, R., Hossain, M.B. & Billah, M. 2016. Fabrication and characterization of aluminum-rice husk ash composite prepared by stir casting method. Rajshahi University Journal of Science and Engineering, 44:9-18.

[4] V. E. Ezechukwu., C. C. Nwobi-Okoye, I. U. Onyenanu Analysis of Waste Gases at INTAFACT Beverages, Onitsha - Nigeria. Journal of Emerging Technologies and Innovative Research Volume 2 Issue 10 November 2015 eISSN: 2349-5162

[5] Aigbodion, V., Bean pod ash nanoparticles a promising reinforcement for aluminum matrix biocomposites. Journal of Materials Research and Technology, 2019. 8(6): p. 6011-6020.

[6] Ni DR, Wang JJ, Zhou ZN, Ma ZY. Fabrication and mechanical properties of bulk NiTip/Al composites prepared by friction stir processing. Journal of Alloys and Compounds 2014;586:368-74.

[7] Moghaddas MA, Bozorg SFK. Effects of thermal conditions on microstructure in the nanocomposite of Al/Si3N4 produced by friction stir processing. Mater Sci Eng A 2013;559:187-93.

[8] Liu ZY, Xiao BL, Wang WG, Ma ZY. Analysis of carbon nanotube shortening and composite strengthening in carbon nanotube/aluminum composites fabricated by multi-pass friction stir processing. Carbon 2014;69:264-74.

[9] Hashemi R, Hussain G. Wear performance of Al/TiN dispersion strengthened surface composite produced through friction stir process: A comparison of tool geometries and several passes. Wear 2015;324-325:45-54.

[10] Sharifitabar M, Sarani A, Khorshahian S, Afarani MS. Fabrication of 5052Al/Al2O3 nanoceramic particle reinforced composite via friction stir processing route. Mater Des 2011;32:4164-72.

[11] Thangarasu A, Murugan N, Dinaharan I, Vijay SJ. Synthesis and characterization of titanium carbide particulate reinforced AA6082 aluminum alloy composites via friction stir processing. Arch Civ Mech Eng 2015; 15:324-34.

[12] Yadav D, Bauri R. Nickel particle embedded aluminum matrix composite with high ductility. Mater Lett 2010; 64:664-7.

[13] Ezeugo , J. O., Onukwuli , O. D., Ikebudu , K. O., Ezechukwu , V. C., & Nwaeto , L. O. (2019). Investigation of Akuamma Seed Extract on Corrosion Inhibition of Aluminum in Hydrochloric Acid Pickling Environment. Earthline Journal of Chemical Sciences, 1(2), 115-138. https://doi.org/10.34198/ejcs.1219.115138

[14] Raaft M, Mahmoud TS, Zakaria HM, Khalifa TA. Microstructural, mechanical, and wear behavior of A390/graphite and A390/Al2O3 surface composites fabricated using FSP. Mater Sci Eng A 2011; 528:5741-6.

[15] Akinwamide, S.O., Akinribide, O.J. & Olubambi, P.A. 2021. Microstructural evolution, mechanical and nanoindentation studies of stir cast binary and ternary aluminum-based composites. Journal of Alloys and Compounds, 850:156586.

[16] Ngu, P. Z. Z., Chia, S. P. P., Fong, J. F. Y., & Ng, S. M. (2016). Synthesis of carbon nanoparticles from waste rice husk used for the optical sensing of metal ions. New Carbon Materials, 31(2), 135-143. doi:10.1016/s1872-5805(16)6000

[17] Asafa, T., Durowoju, M., Oyewole, A., Solomon, S., Adegoke, R. & Aremu, O. 2015. Potentials of Snailshell as a Reinforcement for Discarded Aluminum Based Materials. International Journal of Advanced Science and Technology, 84:1-8.

[18] Dagwa, I. M., & Adama, K. K. (2018). Property evaluation of pumice particulate-reinforcement in recycled beverage cans for Al-MMCs manufacture. Journal of King Saud University - Engineering Sciences, 30(1), 61-67. doi: 10.1016/j.jksues.2015.12.00

[19] Ezechukwu, V. C., Nwobi-Okoye, C. C., Atanmo, P. N., & Aigbodion, V. S. (2020). Wear performance of value-addition epoxy/breadfruit seed shell ash particles and functionalized momordica angustisepala fiber hybrid composites. Revue des Composites et des Materiaux Avances, 30(5), 195-202. https://doi.org/10.18280/rcma.305-601

[20] Yerinmearede, Erebugha & Chinedu, Kennedy & Chukwuemeka, Ezechukwu. (2023). Green Plants Extracts Corrosion Inhibition of Aluminum -A Review. 7. 8-15.

[21] Chukwuemeka, Ezechukwu. (2024). Hybridization Effect on Thermo-mechanical Behaviour of Epoxy/breadfruit Seed Shell Ash Particles and Momordica Angustisepala

Fiber Composites for High- temperature Devices Application. Proceedings of the IRE. Volume 7. 2456-8880. https://www.irejournals.com/formatedpaper/1705783.pdf

[22] Ezeugo, J.O., Onukwuli, O.D., Ikebudu, K.O., Ezechukwu, V.C., & Nwaeto, L. (2019). Optimization of Chrysophyllum albidum leaf extract as corrosion inhibitor for aluminium in 0.5 M H2SO4.

[23] T.T. Braide, C.C. Nwobi-Okoye, V.C. Ezechukwu, Microstructural and Electrochemical study of Value-added Al-Si-Mg alloy reinforced with synthesis carbon nanotube and periwinkle shell nanoparticles for brake disc application, Chemical Data Collections, Volume 39,2022,100878, ISSN 2405-8300, https://doi.org/10.1016/j.cdc.2022.100878. (https://www.sciencedirect.com/science/article/pii/S2405830022000519)

[24] Yerinmearede, Erebugha & Chinedu, Kennedy & Chukwuemeka, Ezechukwu. (2024). CORROSION INHIBITION OF DENNETTIA TRIPETALA ON ALUMINUM IN ALKALINE (NaOH) SOLUTION MEDIUM. International Research Journal of Modernization in Engineering Technology and Science. 6. 3565-3573. 10.56726/IRJMETS48913.

[25] V. E. Ezechukwu., C. C. Nwobi-Okoye, I. U. Onyenanu Analysis of Waste Gases at INTAFACT Beverages, Onitsha - Nigeria. Journal of Emerging Technologies and Innovative Research Volume 2 Issue 10 November-2015 eISSN: 2349-5162 [26] Abdelmalik, A. A., & Sadiq, A. (2019). Thermal and electrical characterization of composite metal oxides particles from the periwinkle shell for a dielectric application. SN Applied Sciences, 1(4). doi:10.1007/s42452-019-0388-5

[26] Ajala E.O., Eletta. O.A.A., Ajala. M.A and Oyeniyi. S.K. Characterization and Evaluation of Chicken Eggshell for use as a Bio-Resource, Arid Zone Journal of Engineering, Technology, and Environment, March 2018; Vol. 14(1):26-40

[27] Muhammad Asnawi, Saman Azhari, Mohd Nizar Hamidon, Ismayadi Ismail, and Intan Helina Synthesis of Carbon Nanomaterials from Rice Husk via Microwave Oven, Journal of Nanomaterials Volume 2018, Article ID 2898326, 5 pages https://doi.org/10.1155/2018/2898326

[28] Ezechukwu, V.C., Nwobi-Okoye, C.C. & Atanmo, P.N. Surface modification of Momordica angustisepala fiber using temperature-activated amino-functionalized alkali-silane treatment. Int J Adv Manuf Technol 109, 1397-1407 (2020). https://doi.org/10.1007/s00170-020-05697-w

[29] Selvan, B. M. M., Anandakrishnan, V., Duraiselvam, M., Venkatraman, R., & Sathish, S. (2018). Multi-Objective Optimization of Wear Behaviour of In Situ AA8011-ZrB2 Metal Matrix Composites by Using Taguchi-Grey Analysis. Materials Science Forum, 928, 162-167. doi: 10.4028/www.scientific.net/msf.928.162